Conf-920375--22

FATIGUE AND ENVIRONMENTALLY ASSISTED CRACKING IN LIGHT WATER REACTORS*

T. F. Kassner, W. E. Ruther, H. M. Chung,
P. D. Hicks, A. G. Hins, J. Y. Park, and W. J. Shack

Materials and Components Technology Division
Argonne National Laboratory
Argonne, Illinois 60439 USA

ANL/CP--76322

DE92 014851

March 1992

DISCLAIMER

For presentation at the NRC Aging Research Information Conference, March 24-27, 1992, Rockville, MD.

---

*Work supported by the Office of Nuclear Regulatory Research, U.S. Nuclear Regulatory Commission FIN Nos. A2?122 and A22562; Program Managers: Drs. J. Muscara and E. Woolridge.

FATIGUE AND ENVIRONMENTALLY ASSISTED CRACKING IN LIGHT WATER REACTORS*

T. F. Kassner, W. E. Ruther, H. M. Chung,
P. D. Hicks, A. G. Hins, J. Y. Park, and W. J. Shack

Materials and Components Technology Division
Argonne National Laboratory
Argonne, Illinois 60439 USA

Abstract

Fatigue and stress corrosion cracking (SCC) of low-alloy steel used in piping and in steam generator and reactor pressure vessels have been investigated. Fatigue data were obtained on medium-sulfur-content A533-Gr B and A106-Gr B steels in high-purity (HP) deoxygenated water, in simulated pressurized water reactor water, and in air. Analytical studies focused on the behavior of carbon steels in boiling water reactor (BWR) environments. Crack-growth rates of composite fracture-mechanics specimens of A533-Gr B/Inconel-182/Inconel-600 (plated with nickel) and homogeneous specimens of A533-Gr B steel were determined under small-amplitude cyclic loading in HP water with ≈300 ppb dissolved oxygen. Radiation-induced segregation and irradiation-assisted SCC of Type 304 SS after accumulation of relatively high fluence also have been investigated. Microchemical and microstructural changes in HP and commercial-purity Type 304 SS specimens from control-blade absorber tubes used in two operating BWRs were studied by Auger electron spectroscopy and scanning electron microscopy, and slow-strain-rate-tensile tests were conducted on tubular specimens in air and in simulated BWR water at 289°C.

1 Introduction

Fatigue and environmentally assisted cracking of piping, pressure vessels, and core components in light water reactors (LWRs) are important concerns as reactors age. The degradation processes include intergranular stress corrosion cracking (SCC) of austenitic stainless steel (SS) piping in boiling water reactors (BWRs), and propagation of fatigue or SCC cracks, which initiate in sensitized SS cladding, into low-alloy ferritic steels in BWR

*Work supported by the Office of Nuclear Regulatory Research, U.S. Nuclear Regulatory Commission FIN Nos. A22122 and A22562; Program Managers: Drs. J. Muscara and E. Woolridge.

pressure vessels. Cracking has also occurred in upper shell-to-transition cone girth welds in pressurized water reactor (PWR) steam generator vessels. After accumulation of relatively high fluence reactor-core internal components become susceptible to cracking, which has been attributed to radiation-induced segregation (RIS) of elements such as Si, P, S, Ni, and Cr. Ongoing research at Argonne is addressing these problems.

2 Summary of Research Progress

2.1 Fatigue of Ferritic Steels

Plain carbon and low-alloy steels are used extensively in PWR and BWR nuclear steam supply systems as piping and pressure vessel materials. The steels of interest for these applications include A106-Gr B and A333-Gr 6 for seamless pipe and A302-Gr B, A508-2, and A533-Gr B plate for pressure vessels. The current Section III fatigue curves for carbon and low-alloy steels are based on tests in air at room temperature.[1] Tests in air at reactor operating temperatures fall below the ASME mean-data curve in portions of the low cycle regime.[2] However, in oxygenated water at low strain rates, the fatigue lives of carbon steels are decreased markedly, and specimen data can fall below the ASME Section III Design Curve.[3-8] Iida et al.[7] and Higuchi and Iida[8] studied the fatigue of A508-Cl3 and A333-Cl6 in deionized water at temperatures up to 290°C. They also showed that in oxygenated water at large strain amplitudes, fatigue lives were reduced in tests at lower strain rates. The magnitude of the decrease depended strongly on alloy composition, temperature, and concentration of dissolved oxygen in the water. At dissolved-oxygen concentrations of <100 ppb, the aqueous environment had little effect on the fatigue life of either alloy.

Nagata et al.[9] performed fatigue tests on forged ASTM A508 Cl-3 and on the rolled-equivalent ASTM A533-Gr B Cl-1 under strain control (at various strain rates) in pure water at several dissolved-oxygen levels. Compared to tests in air, water containing 100 ppb dissolved oxygen had very little effect on the fatigue behavior of either alloy at a strain rate of 1×10^{-3} s^{-1}. However, a decrease in strain rate by up to two orders of magnitude decreased the fatigue life of A533-Gr B steel, whereas A508 steel showed little effect of strain rate. Nagata et al.[9] attributed this to the higher sulfur content of the A533-Gr B steel compared to the A508 material. Terrell[10] performed tests on A106-Gr B in PWR environments. For cyclic frequency in the range of 1.0-0.017 Hz, the fatigue life of smooth test specimens was virtually unaffected by the environment.

Experimental studies have focused on fatigue testing in PWR environments, whereas analytical studies have focused on the behavior of carbon steels in BWR environments.

2.1.1 Experimental Methods

Uniaxial fatigue properties of A533-Gr B pressure vessel and A106-Gr B piping steels in water and in air were investigated. The A533-Gr B material for the test specimens was obtained from the lower head of the Midland Reactor, which was scrapped before the plant was completed. The medium-sulfur (S)-content (0.016% S) steel had a tempered bainitic microstructure in the as-fabricated condition. Chemical analyses (wt.%) of two materials for the fatigue study and the ferritic steel used in crack-growth-rate (CGR) tests are given in Table 1.

Table 1. Chemical Composition (wt.%) of Ferritic and Austenitic Steels for Fatigue[a,b] and Compact Tension Specimens[c]

Material	C	P	S	Si	Fe	Cr	Ni	Mn	Mo	Ta/Nb	Ti
A533-Gr B[a]	0.20	0.014	0.016	0.17	Bal	0.19	0.50	1.28	0.47	-	-
A106-Gr B[b]	0.29	0.014	0.014	0.28	Bal	0.19	0.11	0.92	0.04	-	-
A533-Gr B[d]	0.22	0.012	0.018	0.22	Bal	0.12	0.69	1.45	0.53	-	-
IN-182[e]	0.10	0.03	0.01	1.0	10.0	14.0	65.0	7.0	-	1.75	1.0
IN-600	0.07	-	0.001	0.19	9.41	15.23	73.84	0.30	-	0.12	0.31

[a]Medium-sulfur-content steel for fatigue specimens was obtained from the lower head of the Midland Reactor.

[b]Heat No. J-7201 (20-in.-diameter schedule 140 pipe) fabricated by the Cameron Iron Works, Houston, TX.

[c]Composite Alloy-600/In-182/A533-Gr B compact tension (1T) specimen was fabricated such that the low-alloy steel was in the T-L orientation according to the ASTM nomenclature. Other 1TCT specimens of low-alloy steel were also in the T-L orientation.

[d]A533-Gr B Class 1 plate (Heat No. A-1195-1) was obtained from the Oak Ridge National Laboratory HSST Program.

[e]Nominal composition of undiluted Inconel-182 weld metal (AWS Type ENiCrFe-3 per AWS Specification A5.11). A layer, ≈6 mm thick, was buttered to the A533-Gr B plate with a 3/32-in.-diameter weld rod and the material was heat treated at 621°C for 24 h and air-cooled. Inconel-600 (Heat No. NX5922-G11) was electron-beam-welded to the Inconel-182 to form the 1TCT specimen. Entire specimen was nickel-plated.

Fatigue tests were performed on smooth (1.0-μm surface-polished gage length, 19 mm) cylindrical hourglass-type specimens. The specimens were loaded uniaxially with a triangular wave form at a strain rate of 4×10^{-3} s^{-1}. Tests were first performed in air at 288°C in strain control. Strain ranges of 1.0, 0.75, 0.50, and 0.35% were selected. The stroke response was recorded so that subsequent fatigue tests in water could be run in stroke control. After obtaining the strain control data in air, a repeat test was performed under stroke control in air at 288°C. The mean stroke and stroke amplitude settings for these tests were those obtained at the half-lives of the strain control tests. Excellent agreement was obtained between the tests performed in strain control and those performed in stroke control. Tests were conducted in high-purity (HP) deoxygenated water and in simulated PWR water at a flow rate of 8 $mL \cdot min^{-1}$ in a small autoclave (annular volume of 12 mL) at 288°C and a system pressure of 9 MPa. The nominal water chemistries are given in Table 2.

2.1.2 Results

The fatigue test results are summarized in Tables 3 and 4 and Figs. 1 and 2. The number of cycles to failure (fatigue life N_{25} in Fig. 1) is determined when the tensile stress amplitude decreases to 75% of the value observed at one-half of the fatigue life. The life is plotted in terms the strain range, $\Delta\varepsilon_t$. In Fig. 1, the lives in the environment are compared with the best fit curves for the lives in air. The data can be compared with the ASME Section III mean-data curve and the design fatigue curves for carbon and low-alloy steels.[1]

Table 2. Nominal Water Chemistries for Fatigue Tests

Water Chemistry	Deionized Water	PWR Water
Conductivity ($\mu S \cdot cm^{-1}$)	0.17	25
pH (room temperature)	5.8	6.6
Dissolved O_2 (ppb)	<10	<10
Boron (ppm)	-	1000
Lithium (ppm)	-	2
Chloride (ppm)	<0.03	<0.03
Fluoride (ppm)	<0.01	<0.01
Dissolved H_2 (cm^3/kg)	-	18

Table 3. Test Conditions and Fatigue Lives for A533-Gr B Steel

Test Number	Total Strain Range, $\Delta\varepsilon_t$ (Test Control)	Environment 288°C	Cycles = N_{25}
1505	0.50% (strain)	Air	31,200
1508	1.00% (strain)	Air	3,305
1515	0.75% (strain)	Air	6,792
1517	0.35% (strain)	Air	2,053,295
1522	≈0.89% (stroke)	Air	3,419
1523	≈0.90% (stroke)	Air	2,200
1524	≈0.94% (stroke)	Air	3,714
1525	≈0.45% (stroke)	Air	65,758
1526	≈0.90% (stroke)	Deionized water	3,330
1527	≈0.45% (stroke)	Deionized water	10,334
1528	≈0.45% (stroke)	Deionized water	25,890
1529	≈0.45% (stroke)	PWR water	31,751
1530	≈0.90% (stroke)	PWR water	1,355
1533[a]	≈0.90% (stroke)	PWR water	3,416
1538	≈0.39% (stroke)	Air	>1,000,000
1539	≈0.39% (stroke)	PWR water	136,969
1542	≈0.39% (stroke)	PWR water	>1,154,892
1545	≈0.91% (stroke)	PWR water	3,264

[a]Positive sawtooth test: tensile-going strain rate of 4×10^{-5} s^{-1} (slower by 100X than the other tests) and a compression-going rate of 4×10^{-3} s^{-1}.

Table 4. Test Conditions and Fatigue Lives for A106-Gr B Steel

Test Number	Total Strain Range, $\Delta\varepsilon_t$ (Test Control)	Environment 288°C	Cycles = N_{25}
1498	1.00% (strain)	Air	1,051
1543	0.50% (strain)	Air	14,525
1546	≈1.03% (stroke)	Air	1,365
1547	≈1.03% (stroke)	PWR water	692
1548	0.50 % (stroke)	Air	10,632
1549	0.50% (stroke)	PWR water	9,396
1552	0.35 % (strain)	Air	93,322
1553	0.75% (strain)	Air	3,253

[a]Positive sawtooth test with a tensile-going strain rate of 4 x 10^{-3} s^{-1}.

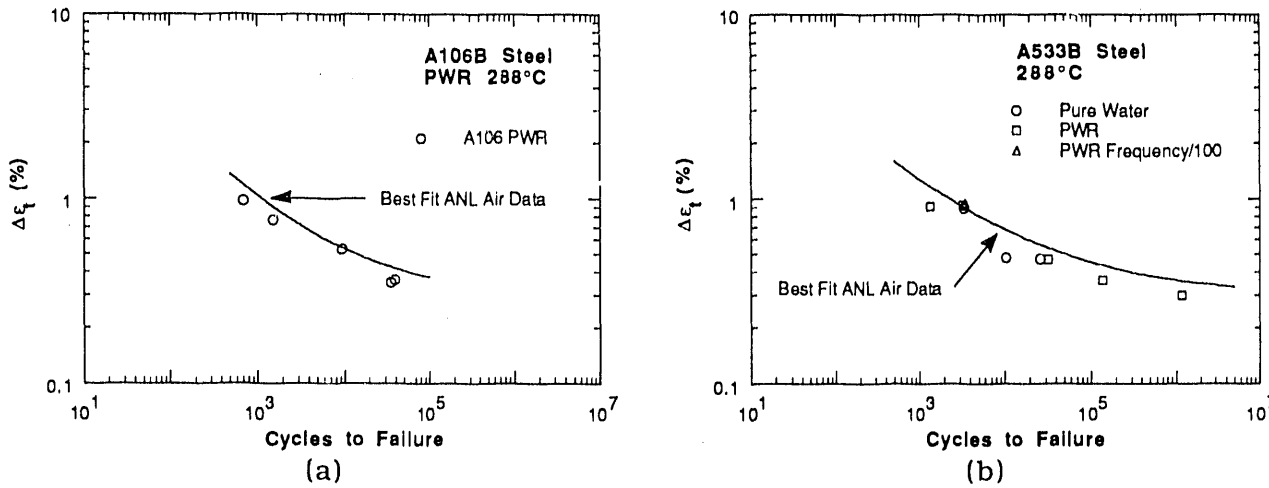

Figure 1. Comparison of lives obtained in deoxygenated water at 288°C with the best-fit curves for corresponding tests in air

The fatigue data for A106-Gr B steel in deoxygenated environments fall only slightly below the best-fit curve in air. The data for the A533-Gr B steel appear to fall somewhat lower than the air curve, but at least based on the one test at a strain rate of 4 x 10^{-5} s^{-1}, life does not appear to decrease with decreasing strain rate, as was observed in tests in oxygenated environments.[7,8] Our results are consistent with those of Iida et al.,[7] Nagata et al.[9], Terrell,[10] Prater and Coffin[11,12] where the effects of environment were minimal at dissolved-oxygen levels of <100-200 ppb. Data at higher stress amplitudes tend to fall further below the ASME mean-data curve than data at longer lives, which is also consistent with the results of Terrell.[10]

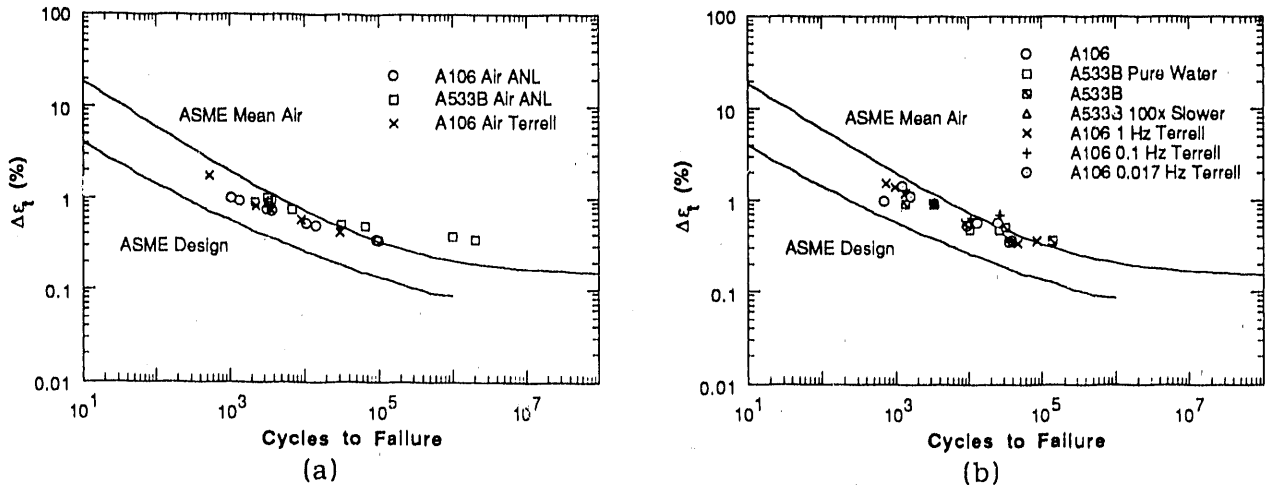

Figure 2. Comparison of ANL data in air and in deoxygenated water with ASME Section III mean air and design curves, and with data of Terrell[10]

2.1.3 Fracture Mechanics Model for the Prediction of Fatigue Lives Based on Crack Growth Rate

An alternative approach to the development of fatigue-life curves is based on the application of fracture-mechanics CGR calculations to predictions of low-cycle fatigue life. In the low-cycle fatigue regime (relatively high strain ranges), fatigue life is controlled primarily by crack growth. Dowling[13] has demonstrated that by characterizing the fracture-mechanics CGR in terms of ΔJ, fracture-mechanics analyses can be used to develop estimates of fatigue-life curves in the low-cycle regime where fatigue life is dominated by crack growth.

The crack growth approach is strictly applicable only when fatigue life is dominated by crack growth. By comparing lives predicted by the crack growth model with actual fatigue lives in air, an estimate of the cycles required to initiate fatigue cracks can be obtained. Because expected life at high strain ranges is dominated by crack growth, life at low strain ranges is dominated by initiation. Fatigue lives in a reactor environment were calculated based on the **assumption** that the number of cycles required to initiate cracks was unaffected by the environment. The crack growth curves for low-alloy steels recently proposed for inclusion in Section XI of the ASME Code,[14] which are based primarily on test data on low-alloy steels, were assumed to be applicable to carbon steels.

The fatigue-life curves developed by this approach (Fig. 3) show a decrease in life with strain rate similar to that observed in conventional fatigue tests in aqueous environments. However, because there is a threshold CGR for environmental enhancement, the crack growth model, unlike the empirical correlations presented in Refs. 7 and 8, does not show a monotonic decrease with decreasing strain rate. A critical strain rate is predicted below which fatigue lives increase. This critical strain rate is a function of strain range, as shown in Fig. 4. Such a saturation appears to have been observed in Russian work[15] in simulated BWR environments at about the strain rates predicted by the model.

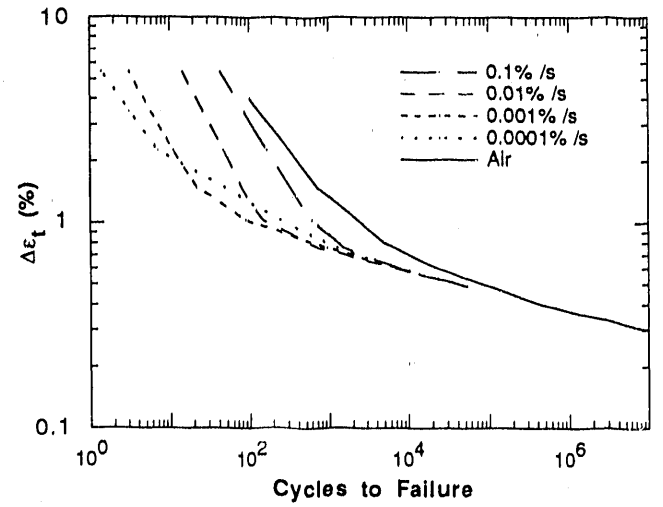

Figure 3.
Fatigue-life curves predicted by crack growth model assuming no effect of environment on initiation

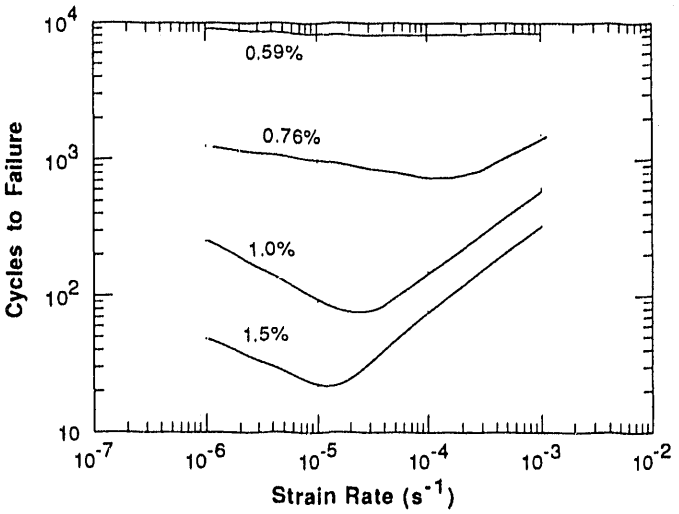

Figure 4.
Fatigue life as a function of strain rate predicted by crack growth model

Above the critical strain rate, the model predicts that lives will decrease with decreasing strain rate in a power-law fashion as assumed in the correlation developed by Higuchi and Iida.[8] However, the empirical correlation assumes that this power-law dependence is independent of strain range. The crack growth model predicts that the strain-rate exponent p (determined from the slope of fatigue-life-versus-strain-rate plots at strain rates above the critical value) is dependent on the strain range. For high strain ranges where life is dominated by crack growth, p is independent of strain range, but at lower strain ranges, it decreases rapidly. The numerical value determined from the crack growth model at high strain ranges, p = 0.61, is close to that obtained from the correlations of Ref. 8 for 0.2 ppm dissolved oxygen at 288°C, i.e., 0.65. The sharp decrease in p at lower strain ranges is due to the **assumption** that the initiation life is unaffected by the environment. Because the crack growth curve used in the analysis is assumed to be valid for both PWR and BWR environments, this model suggests that environmental effects on fatigue life should be significant in PWR environments also, which contradicts fatigue data in these environments

presented in the previous section as well as other reported data.[7-12] The discrepancy may be due to the greater difficulty of actually achieving high environmental CGRs in PWR environments in situations without a deep crack to provide a crevice chemistry.

The model suggests that a correlation of the form

$$p = p_o + M(O)\cdot N(T)\cdot F(\Delta\varepsilon) \qquad (1)$$

where $\Delta\varepsilon$ is the strain range and

$$F(\Delta\varepsilon) = f_o\left(\frac{\Delta\varepsilon}{0.01}\right)^n \qquad \Delta\varepsilon < 0.01$$
$$= f_o \qquad \Delta\varepsilon \geq 0.01 \qquad (2)$$

be considered. Reanalysis of the data in Refs. 3, 6, and 8 confirms that a correlation of the form in Eq. (1) does provide a somewhat better fit to the experimental data. However, the values contradict the prediction of the crack growth model that strain rate sensitivity decreases markedly with decreasing strain range. The empirical data indicate that the strain rate sensitivity increases with decreasing strain range. Similar results were observed in the tests reported in Ref. 15.

2.2 Stress Corrosion Cracking of Ferritic Steels

Over the past 15 years, the corrosion fatigue properties of low-alloy steels in LWR primary-system water chemistries have been studied extensively.[16-19] Much less information is available on SCC of these materials.[20-24] Because it is clear that very high CGRs can occur in some materials under some combinations of loading and environment, the objective of the current work is to better define the circumstances that can produce SCC in these steels.

2.2.1 Experimental Methods

Fracture-mechanics CGR tests have been carried out on a heat of medium-sulfur-content (0.018 wt.%) A533-Gr B pressure vessel steel (chemical composition is given in Table 1). In addition to conventional 1-T compact-tension specimens, specimens plated with either nickel or gold, together with a composite specimen of A533-Gr B/Inconel-182/Inconel-600 plated with nickel, were tested. Nickel-plated specimens were used to better simulate a clad ferritic steel vessel, where only the low-alloy steel at the crack surface is exposed to the environment. Surface films on the nickel- and gold-plated specimens are different from those on the nonplated ferritic specimens. Because virtually all of the existing data have been obtained on specimens without cladding, it is important to verify that those results were not unduly affected by the character of the surface film.

The composite specimen was tested in simulated BWR water with ≈200 ppb dissolved oxygen at 289°C under cyclic loading with a positive sawtooth wave form (12-s loading and 1-s unloading times) at 0.08 Hz, load ratios ($R = K_{min}/K_{max}$) of 0.9 to 1.0, and maximum stress intensities, K_{max}, of ≈28 to 62 MPa·m$^{1/2}$. Crack-length measurements in conventional and plated specimens were made by a DC-potential-drop technique. Because

no potential-drop calibration was available for the composite specimen, crack length was measured by the compliance method.

2.2.2 Results

Results from SCC tests on the composite specimen are given in Table 5. The fatigue precrack in the specimen traversed the Inconel-182 weld metal so that the initial 7.2 mm of crack growth over a time interval of 1000 h (Test 1) occurred in the underlying A533-Gr B material at an average rate of 2.0×10^{-9} m·s^{-1}. The K_{max} increased from 28 to 35 MPa·m$^{1/2}$. No periods of crack arrest or transient crack growth occurred during this phase of the test. This CGR is virtually identical to the "average" value for a previous composite specimen (2.3×10^{-9} m·s^{-1}), which included several crack extensions of 1–2 mm within ≈170-h time intervals followed by ≈800-h periods of very slow steady-state growth.[25] For no apparent reason, the CGR of the composite specimen in the current test decreased abruptly at ≈1050 h to a very low value that continued over an ≈1000-h time period. This behavior is similar to that observed in the previous experiment.[25]

In Test 2, the K_{max} of the composite specimen was increased to 40 MPa·m$^{1/2}$ at an R of 0.95. Whereas an increase of K_{max} in the previous experiment,[25] in general, resulted in a brief increase in the CGR, no such increase was noted during the next 300-h period in this test. At that period, the dissolved-oxygen concentration in the feedwater was increased to ≈30 ppm (Test 3). This action initiated a return to the high-CGR regime, which we allowed to persist for two weeks. The feedwater was then returned to the normal dissolved-oxygen concentration of ≈0.4 ppm in Test 4, and shortly thereafter, the CGR returned to a low level (7.6×10^{-11} m·s^{-1}) for 800 h. The dissolved-oxygen level was then increased to 6 ppm in Test 5, and two days later rapid crack growth resumed. These experiments indicate that dissolved-oxygen concentration is an important variable at a load ratio of 0.95.

In the next series of tests, the effect of load ratio was investigated. In Test 6, the load ratio was increased from 0.95 to 1.0 (i.e., constant load); and shortly thereafter, the CGR returned to the low level even though the dissolved-oxygen level remained at 6 ppm. The low CGR persisted for an additional 1200 h, after which the dissolved-oxygen level was increased to ≈30 ppm in Test 7. This caused a modest increase in CGR over an additional exposure period of 800 h. The load ratio was then decreased to 0.98 in Test 8 and the CGR decreased slightly during an additional 310-h period. The load ratio was decreased further to 0.95 in Test 9 and the CGR remained at the same low value (3.8×10^{-11} m·s^{-1}) over a 200-h interval. In Test 10, the load ratio was decreased to 0.9, and within 24 h, crack growth resumed a high rate (7.8×10^{-9} m·s^{-1}). The test was terminated after ≈20 h because the crack length exceeded the maximum allowable value. Even at a high K level (62 MPa·m$^{1/2}$), a load ratio of <1 is required to initiate a high CGR. No crack growth occurred in a conventional (nonplated) A533-Gr B specimen at a stress intensity factor of 28.7 MPa·m$^{1/2}$ over the entire ≈6600-h experiment under the different environmental and loading conditions.

The CGR results in Table 5 at different dissolved-oxygen levels and load ratios fall into two ranges; i.e., ≈2 to 8×10^{-11} and ≈2 to 8×10^{-9} m·s^{-1}. High CGRs occurred at an R of 0.95 in water containing 0.3, 6, and 30 ppm dissolved oxygen (Tests 1, 5, and 3,

Table 5. Crack Growth of Inconel-182/A533-Gr B Composite Specimen[a] at Constant Load and under Low-Frequency, High-R Loading[b] in High-Purity Water Containing ≈0.3 to 30 ppm Dissolved Oxygen at 289°C

		Water Chemistry			Electrode Potential		CGR Parameters			
Test No.	Time, h	Cond., $\mu S \cdot cm^{-1}$	pH at 25°C	Oxygen,[c] ppm	304 SS, mV(SHE)	Pt, mV(SHE)	Load Ratio	K_{max},[d] $MPa \cdot m^{1/2}$	ΔK,[e] $MPa \cdot m^{1/2}$	Growth Rate, $m \cdot s^{-1}$
1	0–1058	0.16	6.25	0.3	112	126	0.95	35.0	1.75	2.0×10^{-9}
	1058–2156							37.0	1.85	3.0×10^{-11}
2	2156–2492	0.13	6.20	0.3	49	82	0.95	40.0	2.00	3.0×10^{-11}
3	2492–2827	0.15	6.24	30	260	323	0.95	49.1	2.46	3.1×10^{-9}
4	2827–3666	0.12	6.27	0.4	96	137	0.95	50.5	2.53	7.6×10^{-11}
5	3666–3834	0.15	6.19	5.9	198	231	0.95	58.6	2.93	6.9×10^{-9}
6	3834–5005	0.13	6.36	6	183	204	1.0	59.0	0	2.5×10^{-11}
7	5009–6069	0.17	6.27	30	220	222	1.0	60.0	0	8.1×10^{-11}
8	6069–6379	0.14	6.33	31	205	204	0.98	60.1	1.20	3.8×10^{-11}
9	6379–6573	0.14	6.34	28	223	219	0.95	60.2	3.01	3.8×10^{-11}
10	6573–6592	0.14	6.34	28	220	215	0.90	62.4	6.24	7.8×10^{-9}

[a]Composite compact tension specimen (1TCT) (No. 02C-11) was fabricated from Inconel-600/Inconel-182/A533-Gr B Steel (Heat No. A-1195-1). Specimen was electroplated with nickel.

[b]Frequency of the positive sawtooth wave form was 8×10^{-2} Hz; rise-time of 12 s and fall-time of 1 s.

[c]Effluent dissolved-oxygen concentrations below 20 ppm were determined with an Orbisphere dissolved-oxygen meter; higher values were measured with CHEMetrics™ ampules.

[d]Maximum stress intensity, K_{max}, value at the end of each time period.

[e]$\Delta K = K_{max}(1 - R)$, where the load ratio $R = K_{min}/K_{max}$.

respectively). Low CGRs were also measured at this R value in water containing ≈0.3–0.4 and 28 ppm dissolved oxygen (Tests 2, 4, and 9). As mentioned previously, under constant load (R = 1.0), an increase in the dissolved-oxygen concentration from 6 to 30 ppm produced a relatively small increase in the CGRs (Tests 6 and 7). A significant decrease in the load ratio from 1.0 to 0.9 (sequentially in Tests 7–10) caused an abrupt transition to the high-CGR regime at an R of 0.9 in water containing ≈30 ppm dissolved oxygen.

These results along with those from a previous composite specimen in which unusually large jumps in crack length (≈1–2 mm) occurred whenever K_{max} was increased (followed by periods of relatively slow crack growth),[25] indicate that triggering events in the

environment and/or in the loading conditions can produce abrupt changes in the CGRs by two orders of magnitude. For example, increases in dissolved-oxygen concentration and K_{max} and decreases in load ratio can lead to high CGRs. Conversely, a transition from the high- to low-CGR regime can occur by decreasing the dissolved-oxygen concentration or by increasing the load ratio. However, steady-state CGRs can lie in either the high- or low-CGR regime for any given set of loading or environmental conditions. This is illustrated in Fig. 5, which summarizes the results in Table 5 at an R of 0.95 for composite specimen 02C-11, the composite specimen (02C-1) from a previous experiment,[25] and data from gold-plated and nonplated specimens of the same heat of ferritic steel.[25]

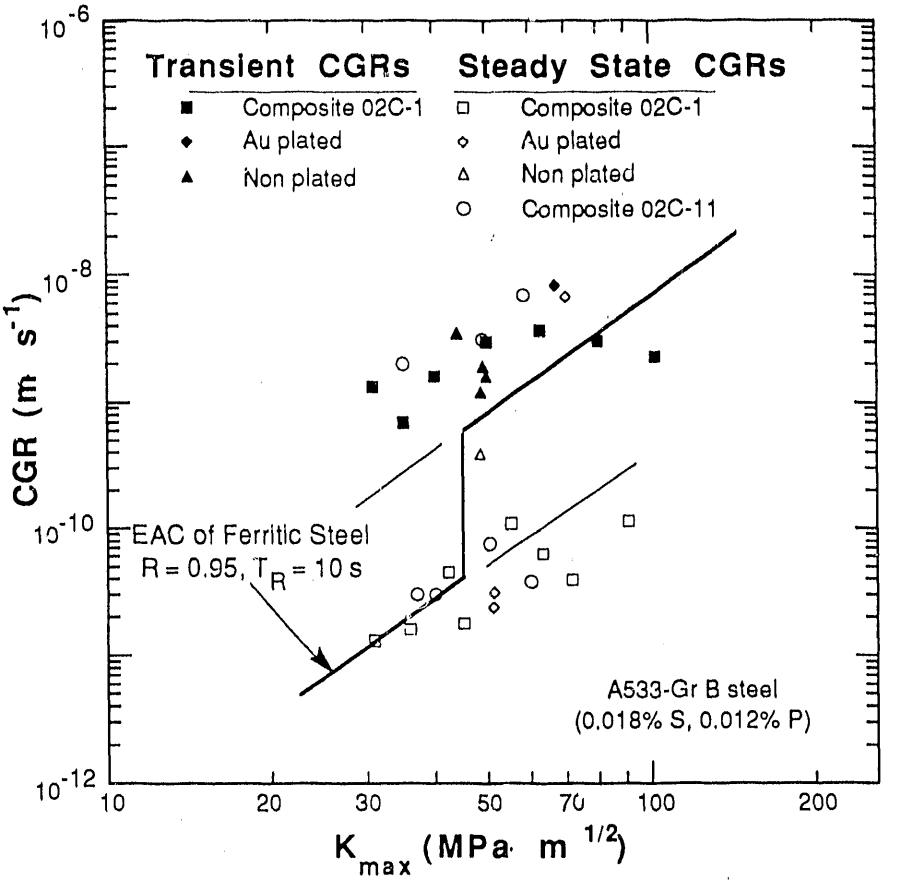

Figure 5. CGRs of A533-Gr B steel under R = 0.95 loading in HP oxygenated water at 289°C vs. K_{max}. Heavy line represents predicted behavior from a modified version of Section XI of the ASME code.

The heavy lines in Fig. 5 represent the predicted dependence of CGR on K_{max} for ferritic steels in 289°C water at an R of 0.95 and a rise-time T_R of 10 s, according to the fatigue CGR curves for ferritic steels in LWR environments proposed for inclusion in Section XI of the ASME code.[14] The model predicts a threshold for a transition from a low, nonenvironmentally assisted CGR to a much higher rate. The threshold K_{max} predicted by

the model (which includes high-oxygen environments that may be more aggressive than those used in tests on which the model is based) is somewhat higher than the present data would indicate. The persistence of low CGRs above the "threshold" is consistent with a hysteresis observed in similar tests at lower R values in other investigations. One can "move up" the lower curve above the threshold without triggering high CGRs, but once high rates are achieved they persist at lower K_{max} levels. The interpretation of the present tests in terms of the threshold model is complicated because we have not run "classical" threshold tests with a fixed environment and a fixed R. The threshold is a function of R and probably of oxygen level. Instead of the single illustrative curve shown in Fig. 5, there should be a family of curves corresponding to the different conditions. The single curve is representative but not necessarily predictive.

The upper-bound values for the experimental data in the high- and low-CGR regimes are $\approx 2 \times 10^{-9}$ and 2×10^{-11} m·s^{-1} (≈2.5 and 0.025 in.·yr^{-1}), respectively, at a K_{max} value of 35 MPa·m$^{1/2}$ Crack-growth rates in the upper regime are clearly unacceptable. The nature of the transitions between the two regimes and the observation that the initial fatigue crack in companion nonplated specimens did not propagate will be investigated further in future experiments.

2.3 RIS and IASCC of HP and CP Type 304 SS from BWR Control-Blade Absorber Tubes

In recent years, failures of reactor-core internal components in both BWRs and PWRs have increased after accumulation of relatively high fluence (>5 x 10^{20} n·cm^{-2}, E >1 MeV). The general pattern of the observed failures indicates that as nuclear plants age and neutron fluence increases, various apparently nonsensitized austenitic materials become susceptible to intergranular failure. Some components are known to have cracked under minimal applied stress. Although most failed components can be replaced, some safety-significant structural components, such as the BWR top guide, shroud, and core plate, would be very difficult or impractical to replace. Therefore, structural integrity of these components after accumulation of high fluence has been a subject of concern, and extensive research has been conducted to provide an understanding of this type of degradation, commonly termed irradiation-assisted stress corrosion cracking (IASCC).[26-43]

Most of the safety-significant structural components are fabricated from solution-annealed austenitic SSs, primarily commercial-purity Type 304 SS. Component fabrication procedures and reactor operational parameters, such as neutron flux, fluence, temperature, water chemistry, residual stress, and mechanical loads, have been reported to influence susceptibility to IASCC.[26-37] However, results from research at several laboratories on materials irradiated under a wide variety of simulated conditions are often inconsistent and conflicting as to the influence of these parameters.[29,36]

Failures of austenitic SS after accumulation of high fluence have been attributed to irradiation-induced segregation (RIS) or depletion of elements such as Si, P, S, Ni, and Cr at grain boundaries. It is generally believed that the nonequilibrium process of RIS of impurity or alloying elements is strongly influenced by irradiation temperature and fast-neutron dose rate. However, the exact identity of the elements that segregate and the extent to which RIS contributes to the enhanced susceptibility of the core-internal components of LWRs to IASCC are not clear. This is particularly true for Type 304 SS, from which majority of the

safety-significant in-core components have been fabricated, although analyses of RIS of impurity elements and grain-boundary depletion of Cr have been reported for Type 304 SS specimens irradiated under simulated conditions, i.e., either in test reactors,[30,31,33] by electrons,[30] or ions.[35,37]

In view of the strong influence of irradiation temperature and dose rate, results obtained from specimens irradiated in test reactors and accelerators must be considered as tentative, and benchmark analyses on actual reactor components must be obtained. For this purpose, high- and commercial-purity (HP and CP) Type 304 SS specimens obtained from neutron absorber tubes of two operating BWRs were analyzed by Auger electron spectroscopy (AES) previously.[41,42] HP Type 304 SS has been suggested as an alternative to CP Type 304 SS. In-reactor and laboratory experience[27,28,34] indicate better IASCC performance of an HP heat of Type 348 SS than of a CP heat of Type 348 SS. Auger analyses of specimens from a CP Type 304 SS neutron absorber rod, revealed significant segregation of Si, P, Ni, and an unidentified element or compound that gives rise to an Auger energy peak at 59 eV.[41,42] Such segregation was negligible in HP material, except for Ni. No evidence of S segregation was observed in either material. However, Cr depletion was more pronounced in the HP material than in the CP material.

The results of the AES analyses of irradiation-induced grain-boundary segregation of impurity and alloying elements have been correlated with SCC susceptibility information from slow-strain-rate-tensile (SSRT) tests on specimens from neutron-absorber-rod tubes to provide insight into mechanism(s) of IASCC.

2.3.1 Experimental Methods

SSRT tests were conducted on a 12 specimens of CP and HP neutron-absorber-rod tubes in air and in simulated BWR water at 289°C to determine tensile properties and IASCC susceptibility as a function of neutron fluence. The chemical compositions of the HP and CP heats are given in Table 6. The dissolved-oxygen concentration and conductivity of the simulated BWR water were ≈280 ppb and 0.13 $\mu S \cdot cm^{-1}$, respectively. SEM fracture surface maps of the SSRT specimens were also obtained. SEM fractography was conducted at a magnification of 125X, and an entire fracture-surface composite was constructed for each specimen to determine the fraction of intergranular, transgranular, and ductile failure.

2.4.2 Results

Test conditions, SSRT data, and SEM analyses of the 12 specimens are summarized in Table 7. Stress-versus-elongation curves from HP and CP specimens tested in simulated BWR water are shown in Fig. 6. From the figure, relative characteristics of stress corrosion of the HP and CP specimens can be deduced. At all fluence levels, the total elongations of the HP specimens were lower than those of the CP heat, indicating a higher SCC susceptibility of the HP material. For example, at a fluence level of 0.6 to 0.7 x 10^{21} $n \cdot cm^{-2}$ (Fig. 6B), the total elongation of the HP specimen was ≈1.8% compared to ≈8.3% of the CP specimen.

Table 6. Chemical Composition (wt.%) and Fast-Neutron Fluence of Irradiated Type 304 SS BWR Absorber-Rod Cladding

Material	Fluence Level, 10^{21} n·cm^{-2}	Specimen Code	Composition (wt.%)									
			Cr	Ni	Mn	C	N	B	Si	P	S	O
HP-304 SS[a]	1.4	VH-A7A	18.50	9.45	1.53	0.018	0.100	<0.001	<0.03	0.005	0.003	-
HP-304 SS[a]	0.7	VM-D5B	18.58	9.44	1.22	0.017	0.037	0.0002	0.02	0.002	0.003	-
HP-304 SS[a]	0.2	VL-A4C			same	as	VH-	A7A				
CP-304 SS[b]	2.0	BL-BWR-2H	16.80	8.77	1.65	0.08[c]	0.052	-	1.55	0.045[c]	0.030[c]	0.024
	0.6	BL-BWR-2M										
	0.2	BL-BWR-2L										

[a]HP neutron-absorber tubes, 4.78-mm-OD, 0.63-mm-wall; composition measured before service.
[b]CP neutron-absorber tube, 4.78-mm-OD, 0.79-mm-wall; composition measured after service.
[c]Represents maximum value in the specification; actual value not measured.

Table 7. Slow Strain Rate[a] Tensile Test Results on Irradiated CP and HP Type 304 SS in Air and in HP Water Containing ≈280 ppb Dissolved Oxygen at 289°C

Absorber Rod Specimen No.	Hot-Cell Identification No.	Fast-Neutron Fluence, n·cm^{-2}	SSRT No.	Feedwater Chemistry			SSRT Parameters				
				Oxygen Conc., ppb	Cond. at 25°C, μS·cm^{-1}	pH at 25°C	Failure Time, h	Maximum Stress, MPa	Total Elong., %	TGSCC, %	IGSCC, %
BL-BWR-2H	389E3A	2.0×10^{21}	IR-9	b	b	b	228	631	13.5	0	0
BL-BWR-2H	389E3D	2.0×10^{21}	IR-12	300	0.13	6.27	21	415	1.2	8	28
BL-BWR-2M	389E2D	0.6×10^{21}	IR-3	b	b	b	580	465	34.8	0	0
BL-BWR-2M	389E2A	0.6×10^{21}	IR-8	290	0.15	6.32	140	359	8.3	55	0
BL-BWR-2L	389E1A	0.2×10^{21}	IR-2	b	b	b	260	390	15.6	0	0
BL-BWR-2L	389E1D	0.2×10^{21}	IR-1	280	0.13	6.23	107	337	6.7	43	0
VH-A7A-L2	406A1F	1.4×10^{21}	IR-5	b	b	b	93	786	5.6	0	0
VH-A7A-L1	406A1E	1.4×10^{21}	IR-4	280	0.10	6.28	11	417	0.6	2	58
VM-D5B-L2	406C3	0.7×10^{21}	IR-6	b	b	b	405	684	24.2	-	-
VM-D5B-L1	406C2	0.7×10^{21}	IR-7	280	0.12	6.26	31	552	1.8	8	34
VL-A4C-L2	406B3	0.2×10^{21}	IR-10	b	b	b	231	607	15.7	-	-
VL-A4C-L1	406B2	0.2×10^{21}	IR-11	330	0.14	6.33	77	520	4.6	47	14

[a]Strain rate of 1.65×10^{-7} s^{-1}.
[b]Test in air at 289°C and strain rate of 1.65×10^{-7} s^{-1}.

Figure 7 shows the ultimate tensile strength (UTS) versus fast-neutron fluence (E >1 MeV) of the CP and HP specimens strained to failure in air (from Table 7). The figure contains similar data for CP-grade BWR plate[26] and CP-grade tensile specimens of Types 304 and 304L SS irradiated in the Advanced Test Reactor (ATR) at 300°C.[31] Data obtained from the present CP neutron-absorber tube are consistent with those of other CP materials shown in the figure. However, for a comparable fluence level, the UTS and yield strength of the HP neutron-absorber tube are significantly higher than those of the CP materials. Figure 8 shows the total elongation versus fast-neutron fluence for the HP and CP materials in Fig. 7. Ductility decreases monotonically as fluence increases, apparently leveling out at a fluence level >1.5×10^{21} n·cm^{-2}. All specimens tested in air failed in a ductile manner, and no evidence of intergranular or transgranular fracture was observed. Morphologies of ductile fracture surfaces of the CP and HP materials were somewhat different; however, it is not understood why the HP material is stronger than the CP material.

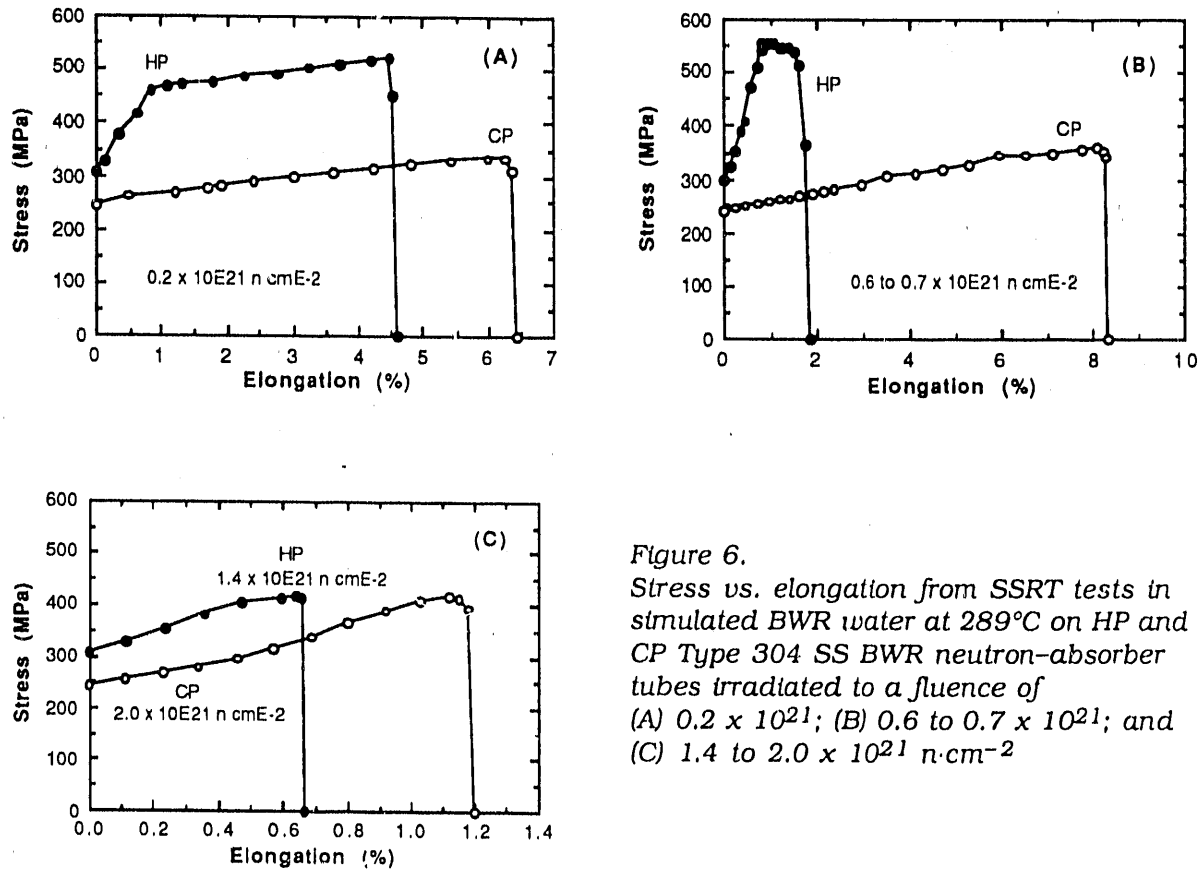

Figure 6.
Stress vs. elongation from SSRT tests in simulated BWR water at 289°C on HP and CP Type 304 SS BWR neutron-absorber tubes irradiated to a fluence of (A) 0.2 x 10^{21}; (B) 0.6 to 0.7 x 10^{21}; and (C) 1.4 to 2.0 x 10^{21} n·cm^{-2}

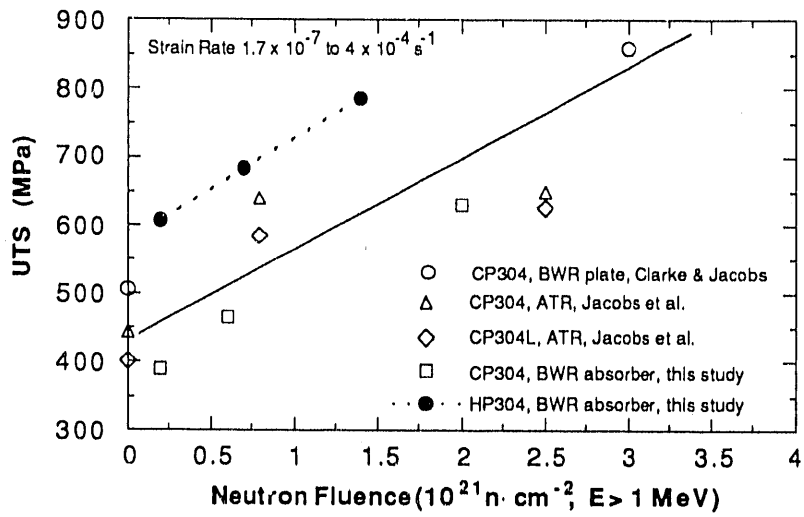

Figure 7. Ultimate tensile stress (UTS) vs. fast-neutron fluence (E >1 MeV) for solution-annealed CP and HP Type 304 SS from tensile tests in air at 289°C

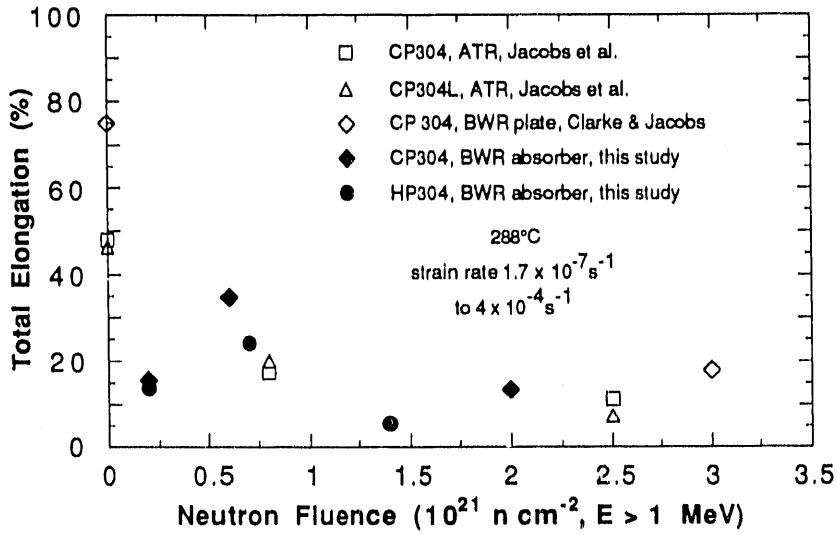

Figure 8. Comparison of total elongation vs. fast-neutron fluence (E >1 MeV) of solution-annealed CP and HP Type 304 SS from tensile tests in air at 289°C

For the three HP and CP SSRT specimens tested in simulated BWR water, the percent IGSCC determined from SEM fractography was, in general, consistent with the decrease in total elongation. This is shown in Fig. 9. Literature data from SSRT tests on Types 304 and 316 SS from CP-grade BWR components are also plotted. The figure indicates that total elongation is also a good measure of IGSCC susceptibility.

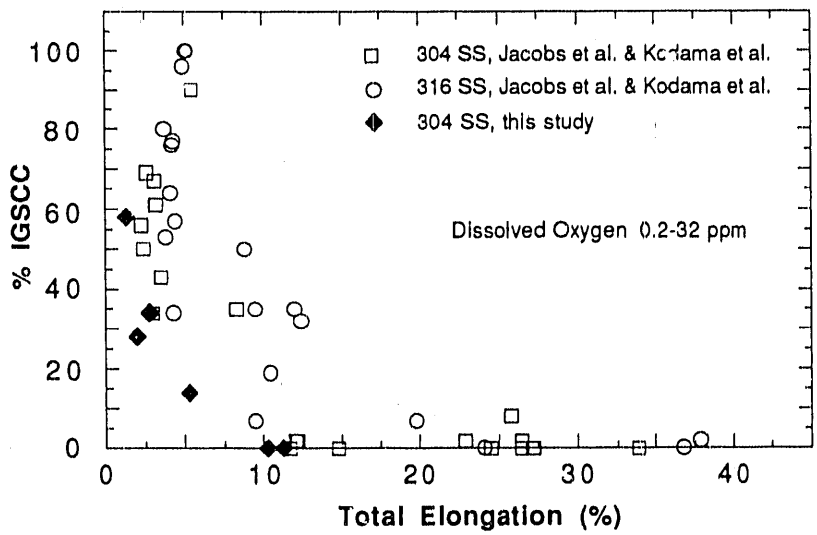

Figure 9. Percent IGSCC vs. total elongation of CP and HP Type 304 SS in the present study and similar data from the literature[31,33,34,43] from SSRT tests at 288°C in simulated BWR water containing 0.2 to 32 ppm dissolved oxygen

The percent IGSCC versus fast-neutron fluence (E >1 MeV) of the present CP and HP heats is shown in Fig. 10, along with similar results from SSRT tests on BWR dry tubes in water containing ≈200 ppb dissolved oxygen reported by Kodama et al.[43] The figure indicates that IGSCC susceptibility of CP material from our neutron-absorber tube and the dry tube is similar at a comparable fluence level, and that the HP material exhibits greater SCC susceptibility. Duplicate tests will be performed on specimens from the HP-grade absorber tube and the CP-grade control-blade-sheath to further confirm the results.

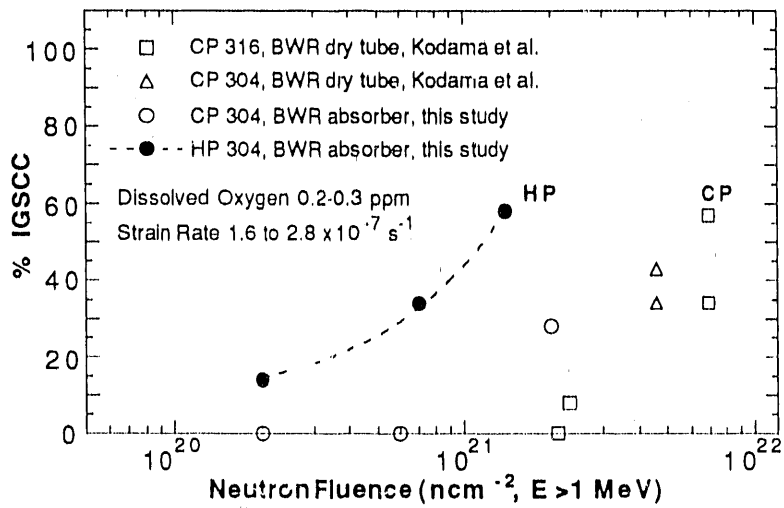

Figure 10. Percent IGSCC vs. fast-neutron fluence (E >1 MeV) for HP Type 304 SS and CP Type 304 and 316 SS[43] from SSRT tests at 288°C in simulated BWR water containing 200-300 ppb dissolved oxygen. HI material exhibits higher susceptibility than CP heats.

3 Conclusions

Fatigue of Ferritic Piping and Pressure Vessel Steels

- The fatigue lives of a medium-sulfur-content A533-Gr B pressure vessel and A106-Gr B piping steels were studied in high-purity deoxygenated water, in simulated PWR water, and in air. Little effect of the environment on fatigue life was observed. Fatigue-life curves based on a fracture mechanics agree well with experimental data at high strain ranges where fatigue life is dominated by crack growth, but underestimate the effect of the environment at lower strain ranges where initiation is important.

Stress Corrosion Cracking of Ferritic Steels

- Fracture-mechanics CGR tests have been performed on composite specimens of A533-Gr B/Inconel-182/Inconel-600 plated with nickel, and on homogeneous specimens of A533-Gr B material plated with gold and nickel. The effects of load history and

dissolved-oxygen content were examined. The CGRs increased markedly during small-amplitude cyclic loading (R = 0.95). Under the cyclic loading, crack growth was observed at K_{max} values that produced no crack growth under constant (R = 1) loading. Under R = 0.95 loading, relatively high CGRs (2×10^{-9} m·s^{-1}) were observed in HP water containing ≈300 ppb dissolved oxygen. When the specimen is in the low-CGR regime (2×10^{-11} m·s^{-1}), increasing the dissolved-oxygen concentration to 6 ppm or higher initiated a return to the high-CGR regime, at least at R value of 0.95.

Irradiation-Assisted Stress Corrosion Cracking of Type 304 SS

- Failures of austenitic SS after accumulation of high fluence have been attributed to radiation-induced segregation (RIS) of elements such as Si, P, S, Ni, and Cr. Microchemical and microstructural changes in high- and commercial-purity (HP and CP) Type 304 SS specimens from control-blade absorber tubes from two operating BWRs were studied by Auger electron spectroscopy and SEM. SSRT tests were conducted on tubular specimens in air and in simulated BWR water at 289°C. Results in air showed that the yield and ultimate tensile strengths of the HP material were higher than those of the CP material for a comparable fluence.

- Stress versus elongation characteristics of the SSRT specimens were consistent with results of SEM analyses of the percent IGSCC on fracture surfaces. IGSCC susceptibility of the present CP absorber tubes was similar to those of other CP heats of Types 304 and 316 SS reported in literature. However, the HP absorber tubes exhibited greater IGSCC susceptibility than did the CP materials.

- It is difficult to explain the relatively high susceptibility of the HP material on the basis of Si or P segregation, because impurity segregation in the HP absorber tubes was negligible for all fluence levels. Rather, the high susceptibility seems to be consistent with the observation that irradiation-induced Cr depletion was more significant in the HP heat than in the CP heat, indicating that irradiation-induced grain boundary depletion of Cr is the primary process in IASCC, at least in simulated BWR water.

References

1. *Criteria of Section III of the ASME Boiler and Pressure Vessel Code for Nuclear Vessels*, The American Society of Mechanical Engineers, United Engineering Center, 345 East Forty-Seventh Street, New York, NY 10017, Library of Congress Catalog No. 56-3934, (1989).

2. J. B Terrell, *Fatigue Life Characterization of Smooth and Notched Piping Steel Specimens in 288°C Air Environments*, NUREG/CR-5013, MEA-2232 (May 1988).

3. D. A. Hale, S. A. Wilson, E. Kiss, and A. J. Gianuzzi, *Low Cycle Fatigue Evaluation of Primary Piping Materials in a BWR Environment*, GEAP-20244, US Nuclear Regulatory Commission (September 1977).

4. D. Hale, S. A. Wilson, J. W. Kass, and E. Kiss, *Low Cycle Fatigue of Commercial Piping Steels in a BWR Primary Water Environment*, J. Eng. Mater. and Technol. **103**, 15–25 (1981).

5. D. Weinstein, *BWR Environment Cracking Margins for Carbon Steel Piping–Final Report*, EPRI Report NP–2046, Electric Power Research Institute, Palo Alto, CA (1982).

6. S. Ranganath, J. N. Kass, and J. D. Heald, Fatigue Behavior of Carbon Steel Components in High–Temperature Water Environments, *Low–Cycle Fatigue and Life Prediction*, ASTM STP 770, C. Amzallag, B. N. Leis, and P. Rabbe, Eds., American Society for Testing and Materials, pp. 436–459 (1982).

7. K. Iida, H. Kobayashi, and M. Higuchi, *Predictive Method of Low Cycle Fatigue Life of Carbon and Low Alloy Steels in High Temperature Water Environments*, NUREG/CP–0067, MEA–2090, Vol. 2 (April 1986).

8. M. Higuchi and K Iida, *Fatigue Strength Correction Factors for Carbon and Low–Alloy Steels in Oxygen–Containing High–Temperature Water*, Nuclear Engineering and Design, **129**, 293–306 (1991).

9. N. Nagata, S. Sato, and Y. Katada, *Low Cycle Fatigue Behavior of Low Alloy Steels in High Temperature Pressurized Water*, Structural Mechanics in Reactor Technol. **10**, 209–214 (1989–8).

10. J. B. Terrell, *Effect of Cyclic Frequency on the Fatigue Life of ASME SA–106–B Piping Steel in PWR Environments*, J. Mater. Eng. **10**, 193–203 (1988).

11. T. A. Prater and L. F. Coffin, *The Use of Notched Compact–Type Specimens for Crack Initiation Design Rules in High–Temperature Water Environments*, Corrosion Fatigue: Mechanics Metallurgy, Electrochemistry, and Engineering, ASTM STP 801, T. W. Crooker and B. N. Leis, eds., American Society for Testing and Materials, Philadelphia, 1983, pp. 423–444.

12. T. A. Prater and L. F. Coffin, *Notch Fatigue Crack Initiation in High Temperature Water Environments: Experiments and Life Prediction*, J. of Pressure Vessel Technol., Trans. ASME, **109**, 124–134 (1987).

13. N. E. Dowling, Crack Growth During Low–Cycle Fatigue of Smooth Axial Specimens, *Cyclic Stress–Strain and Plastic Deformation Aspects of Fatigue Crack Growth*, ASTM STP 637, American Society for Testing and Material, Philadelphia, 1977, pp. 97–121.

14 E. D. Eason, *da/dN Data Analysis Update and Implications for S–N Data Analysis, Presentation at PVRC Workshop Cyclic Life and Environmental Effects in Nuclear Applications*, Clearwater Beach, FL, January 20–21, 1992.

15. V. M Filatov, A. I. Gromova, V. G. Denisov, and V. G. Vasil'ev, *Corrosion Fatigue Test of Steel in Coolant Water*, Ind. Lab. (USSR) **48**, 385–388 (1982). Translated from Zavodskaya Laboratoriya, **48**, 64–67 (1982).

16. P. D. Hicks and F. P. A. Robinson, *Fatigue Crack Growth Rates in a Pressure Vessel Steel under Various Conditions of Loading and the Environment*, Met. Trans. **17A**, 1837-1849 (1986).

17. *Proc. of the Int. Atomic Energy Agency Specialists' Meeting on Subcritical Crack Growth*, NUREG/CP-0044, MEA-2014, Vols. 1 & 2 (May 1983).

18. *Proc. of the 2nd Int. Atomic Energy Agency Specialists' Meeting on Subcritical Crack Growth*, NUREG/CP-0067, MEA-2090, Vols. 1 & 2 (April 1986).

19. *Proc. of the 3rd Int. Atomic Energy Agency Specialists' Meeting on Subcritical Crack Growth*, NUREG/CP-0112, Vols. 1 & 2 (August 1990).

20. T. A. Prater, W. R. Catlin, and L. F. Coffin, *Surface Crack Growth Behavior of Structural Metals in High Temperature Water Environments*, J. Eng. Mater. Technol. **108**, 2-9 (1986).

21. M. O. Speidel and R. M. Magdowski, *Stress Corrosion Cracking of Nuclear Reactor Pressure Vessel Steel in Water: Crack Initiation versus Crack Growth*, Corrosion 88, Paper No. 283, St. Louis, MO (March 1988).

22. D. A. Hale, *The Effect of BWR Startup Environments on Crack Growth in Structural Alloys*, J. Eng. Mater. Technol. **108**, 44-49 (1986).

23. F. P. Ford and P. L. Andresen, *Stress Corrosion Cracking of Low-Alloy Pressure Vessel Steels in 288°C Water*, in Proc. 3rd Int. Atomic Energy Agency Specialists' Meeting on Subcritical Crack Growth, NUREG/CP-0112, Vol. 1, pp. 37-56 (August 1990).

24. P. M. Scott and D. R. Tice, *Stress Corrosion in Low-Alloy Steels*, Nucl. Eng. Des. **119**, 399-413 (1990).

25. T. F. Kassner, W. J. Shack, W. E. Ruther, and J. Y. Park, in *Environmentally Assisted Cracking in Light Water Reactors: Semiannual Report April--September 1990*, NUREG/CR-4667 Vol. 11, ANL-91/9, pp. 3-8 (May 1991).

26. W. L. Clark and A. J. Jacobs, *Effect of Radiation Environment on SCC of Austenitic Materials*, in Proc. 1st Intl. Symp. Environmental Degradation of Materials in Nuclear Power Systems - Water Reactors, National Association of Corrosion Engineers, Houston, pp. 451-461 (1984).

27. F. Garzarolli, D. Alter, and P. Dewes, *Deformability of Austenitic Stainless Steels and Ni-Base Alloys in the Core of a Boiling and Pressurized Water Reactor*, in Proc. 2nd Intl. Symp. Environmental Degradation of Materials in Nuclear Power Systems - Water Reactors, National Association of Corrosion Engineers, Houston, pp. 131-138 (1986).

28. F. Garzarolli, D. Alter, P. Dewes, and J. L. Nelson, *Deformability of Austenitic Stainless Steels and Ni-Base Alloys in the Core of a Boiling and Pressurized Water Reactor*, in Proc. 3rd Intl. Symp. Environmental Degradation of Materials in Nuclear Power Systems - Water Reactors, G. J. Theus and J. R. Weeks, eds., The Metallurgical Society, Warrendale, Pennsylvania, pp. 657-664 (1988).

29. H. Hanninen and I. Aho-Mantila, *Environment-Sensitive Cracking of Reactor Internals*, ibid., pp. 77-92.

30. K. Fukuya, S. Nakahigashi, S. Ozaki, M. Teresawa, and S. Shima, *Grain Boundary Segregation of Impurity Atoms In Irradiated Austenitic Stainless Steels*, ibid., pp. 665-671.

31. A. J. Jacobs, G. P. Wozaldo, K. Nakata, T. Yoshida, and I. Masaoka, *Radiation Effects on the Stress Corrosion and Other Selected Properties of Type-304 and Type-316 Stainless Steels*, ibid., pp. 673-681.

32. E. P. Simonen and R. H. Jones, *Calculated Solute Segregation Kinetics Related to Irradiation Assisted Stress Corrosion Cracking*, ibid., pp. 683-690.

33. A. J. Jacobs, R. E. Clausing, L. Heatherly, and R. M. Kruger, *Irradiation-Assisted Stress Corrosion Cracking and Grain Boundary Segregation in Heat-Treated Type 304 SS*, in Effects of Radiation on Materials: 14th Int. Symp., Vol. I, ASTM STP 1046, N. H. Packan, R. E. Stoller, and A. S. Kumar, eds., American Society for Testing and Materials, Philadelphia, pp. 424-436 (1989).

34. A. J. Jacobs, R. E. Clausing, M. K. Miller, and C. Shepherd, *Influence of Grain Boundary Composition on the IASCC Susceptibility of Type 348 Stainless Steel*, in Proc. 4th Intl. Symp. Environmental Degradation of Materials in Nuclear Power Systems - Water Reactors, National Association of Corrosion Engineers, Houston, pp. 14-21 to 14-45 (1990).

35. C. M. Shepherd and T. M. Williams, *Simulation of Microstructural Aspects of IASCC in Water Reactor Core Components*, ibid., pp. 14-11 to 14-20.

36. P. L. Andresen, F. P. Ford, S. M. Murphy, and J. M. Perks, *State of Knowledge of Radiation Effects on Environmental Cracking in Light Water Reactor Core Materials*, ibid., pp. 1-83 to 1-121.

37. S. Bruemmer, L. A. Charlot, and E. P. Simonen, *Grain Boundary Chemistry Effects on Irradiation-Assisted Stress Corrosion Cracking*, Corrosion 90, Paper No. 506, Las Vegas, NV (April 1990).

38. W. J. S. Yang, *Precipitation Evolution in Type 316 Stainless Steels Irradiated in EBR-II*, in Radiation-Induced Changes in Microstructure: 13th Int. Symp., ASTM STP 955, F. A. Garner, N. H. Packan, and A. S. Kumar, eds., American Society for Testing and Materials, Philadelphia, pp. 628-646 (1987).

DATE
FILMED
7/22/92